Aminated cinnamic acid analogs as dual polarity matrices for high spatial resolution MALDI imaging mass spectrometry

Dufresne, Martin; Migas, Lukasz G.; Djambazova, Katerina V.; Colley, Madeline E.; Van de Plas, Raf; Spraggins, Jeffrey M.

DOI
10.1016/j.aca.2025.344423

Publication date
2025

Document Version
Final published version

Published in
Analytica Chimica Acta

Analytica Chimica Acta 1371 (2025) 344423

Contents lists available at ScienceDirect

Analytica Chimica Acta

journal homepage: www.elsevier.com/locate/aca

Aminated cinnamic acid analogs as dual polarity matrices for high spatial resolution MALDI imaging mass spectrometry

Martin Dufresne [a,b], Lukasz G. Migas [c], Katerina V. Djambazova [a,b], Madeline E. Colley [a,b], Raf Van de Plas [a,c,d], Jeffrey M. Spraggins [a,b,d,e,f,*]

[a] Mass Spectrometry Research Center, Vanderbilt University, Nashville, TN, USA
[b] Department of Cell and Developmental Biology, Vanderbilt University, Nashville, TN, USA
[c] Delft Center for Systems and Control, Delft University of Technology, Delft, Netherlands
[d] Department of Biochemistry, Vanderbilt University, Nashville, TN, USA
[e] Department of Chemistry, Vanderbilt University, Nashville, TN, USA
[f] Department of Pathology, Microbiology, and Immunology, Vanderbilt University, Nashville, TN, USA

HIGHLIGHTS

- Novel dual-polarity MALDI matrices developed for multimodal Imaging MS.
- These compounds are highly sensitive, vacuum stable, low toxicity MALDI matrices.
- Aminated cinnamic acid analogs outperform conventional MALDI matrices.
- ACA minimizes in-source fragmentation for thermally labile molecular species.
- DMACA provided the highest sensitivity enabling routine imaging MS with 5 μm pixels.

GRAPHICAL ABSTRACT

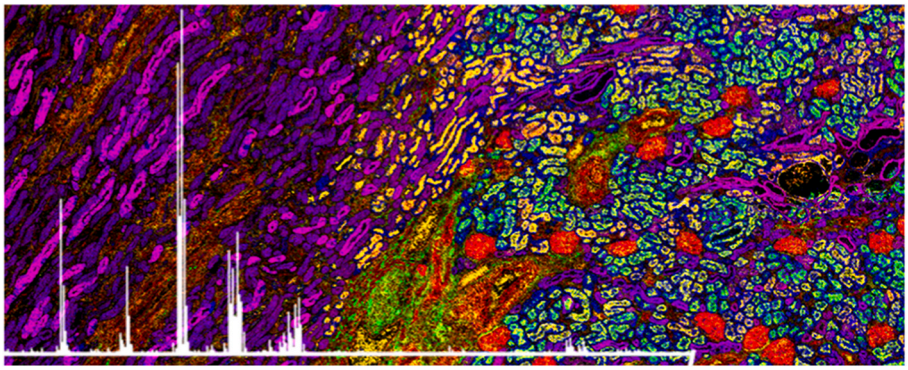

ARTICLE INFO

Handling Editor: Dr. L. Liang

Keywords:
Imaging mass spectrometry
Chemical matrix
Matrix-assisted laser desorption/ionization (MALDI)
4-Dimethylaminocinnamic acid (DMACA)
4-Aminocinnamic acid (ACA)
Lipids

ABSTRACT

Background: We have developed a new class of dual polarity molecules for matrix-assisted laser desorption/ionization (MALDI) imaging mass spectrometry (IMS) capable of acquiring 5 μm pixel sizes with high sensitivity toward polar lipids and metabolites. Aminated cinnamic acid analogs (ACAAs) are vacuum stable, have high extinction coefficients at 355 nm, are highly sensitive to polar lipids, have low toxicity, and are affordable. Current molecules used for high spatial resolution MALDI IMS of polar lipids have shown great success, but are plagued with issues such as low sensitivity at high spatial resolution, vacuum instability, and/or high toxicity. *Results:* ACAAs were evaluated as MALDI matrices, testing them for vacuum stability, absorption at 355 nm, crystal size, sensitivity, and molecular coverage. Among them, 4-aminocinnamic acid (ACA) and 4-(dimethylamino)cinnamic acid (DMACA) were found to perform better than conventional MALDI matrices for lipid IMS experiments. ACA generated fewer in-source fragments due to its high extinction coefficient at 355 nm. This

This article is part of a special issue entitled: Imaging Mass Spectrometry published in Analytica Chimica Acta.

* Corresponding author.Mass Spectrometry Research Center, Vanderbilt University, Nashville, TN, USA.
E-mail address: Jeff.spraggins@vanderbilt.edu (J.M. Spraggins).

https://doi.org/10.1016/j.aca.2025.344423
Received 9 March 2025; Received in revised form 26 June 2025; Accepted 11 July 2025
Available online 15 July 2025

High spatial resolution
timsTOF

leads to better discernment of thermally labile molecules such as gangliosides compared to typical 'soft' ionization matrices like DHA using murine brain tissue. On the other hand, DMACA showed better optical properties than ACA, giving it higher sensitivity from many lipid classes, such as phospholipids and sulfatides. DMACA outperformed DAN and DHA at their individually optimized laser power at small pixel sizes (≤10 μm). DMACA also allows for lower laser power to be used without compromising sensitivity, which reduced the laser spot size at the sample surface from ~6 μm to ~4.5 μm without hardware modifications.

Significance: Improved sensitivity and absorption efficiency at 355 nm allow for 5 μm pixel size MALDI IMS without oversampling while maintaining high S/N on commercial mass spectrometry platforms. Performing MALDI experiments at reduced laser energies minimizes tissue damage, enabling advanced multimodal MALDI IMS studies to be performed on single tissue sections. Comparisons and optimized MALDI IMS methods were performed on murine tissues and human kidney samples as part of the Human Biomolecular Atlas Program.

1. Introduction

Matrix-assisted laser desorption/ionization (MALDI) imaging mass spectrometry (IMS) enables untargeted mapping of a wide range of molecular classes, including drugs, low molecular weight metabolites, lipids, glycans, and proteins [1–5]. The versatility of MALDI IMS stems from its tunable sample preparation protocols, which allow for enhanced detection of specific analyte classes [6–8]. Key factors such as the choice of matrix, the use of tissue washes, the matrix deposition method, and post-matrix application rehydration all significantly impact the ability to image analytes of interest [9–11]. Optimizing these processes has significant impacts on specificity, selectivity, and sensitivity, facilitating highly multiplexed molecular imaging at cellular resolution (≤10 μm pixel sizes) [12]. Other techniques, such as desorption electrospray ionization (DESI) and nanospray DESI (nanoDESI), do not require an additional chemical matrix but are similarly optimized by adjusting tissue washes and extraction solvents. Although great progress has been made in improving spatial resolution for liquid-based surface sampling techniques such as these, MALDI IMS still provides the greatest spatial fidelity, allowing molecular signatures to be precisely linked to specific cell types and tissue structures *in situ* to support biomedical research applications [13–15].

The development of novel MALDI matrices to improve imaging performance has been and continues to be an area of focus for the field. Ideal chemical matrices have a high extinction coefficient for typical MALDI lasers (355 nm), high sensitivity for the targeted analyte class, are vacuum stable, affordable, non-toxic, easy to work with (*e.g.,* easily applied by sprayer or sublimation), and work for both positive and negative ion modes (*i.e.,* dual polarity). Many matrices have been developed that achieve some, but not all, of these figures of merit. For example, 1,5-diaminonapthalene (DAN) is a highly sensitive dual polarity matrix often used for small metabolite and lipid imaging, however, it is known to induce fragmentation and is highly toxic, as it is carcinogenic and mutagenic [9,10,14,16,17]. The Borcher group discovered quercetin as a dual polarity MALDI matrix that yielded good results for many of the figures of merit listed above, but it was not sensitive enough for high spatial resolution experiments [18]. Norharmane was introduced as another candidate matrix by the Ernst group [19,20]. Norharmane has shown great potential providing similar capabilities as DAN in terms of sensitivity, molecular coverage, and vacuum stability, but requires harsh solvents, such as chloroform, to spray properly. It also has poor laser/matrix interaction, necessitating higher laser power, limiting its effectiveness for high spatial resolution experiments and multimodal workflows where minimizing tissue damage is paramount [21,22]. More recently, the Chou group [11] introduced a modified form of anthranilic acid as a dual polarity matrix with similar sensitivity to DAN. They showed that through a simple single methylation of the amino group they could tune the performance of the molecule for MALDI applications, a good example of rational matrix design. This new class of matrix provided good molecular coverage and sensitivity, good laser/matrix interaction with a mid-10^3 $M^{-1}cm^{-1}$ extinction coefficient at 355 nm, and no known toxicity while being relatively inexpensive [10]. Unfortunately, these molecules are highly volatile even in intermediate-pressure MALDI sources, limiting their usability.

Here, we demonstrate the capabilities of a novel, dual polarity class of chemical matrices derived from aminated cinnamic acid and capable of high sensitivity and high spatial resolution MALDI imaging mass spectrometry. These molecules are vacuum stable, have very high extinction coefficients at 355 nm, can be sprayed with non-toxic solvents, can be sublimated, are affordable, and have reported no known toxicity for humans. Using 4-aminocinnamic acid as the core molecule, we synthesized 3 analogs through simple methylation of the amine functional group followed by methylation of the carboxylic acid moiety. This generated 4-(methylamino)cinnamic acid (MACA), 4-(dimethylamino)cinnamic acid (DMACA) and 4-(methylamino)cinnamic methyl ester (TMACA). Each matrix was assessed using a combination of murine and human tissues, highlighting the capability each for high spatial resolution molecular imaging.

2. Materials and methods

2.1. Chemicals and reagents

(E)-4-aminocinnamic acid (ACA) (TCI 98+% purity), 4-dimethylaminocinnamic acid (DMACA) (Thermo Sci 99 % purity), 2,5-dihydroxyacetophenone (DHA) (TCI 98+% purity), norharman (Nor) (Thermo Sci 98 % purity), and 1,5-diaminonaphtalene (DAN) (TCI 98+% purity) were purchased from Fisher Scientific (Pittsburgh, PA). Ammonium sulfate (99+% purity) and all HPLC-grade solvents were purchased from Millipore Sigma (St. Louis, MO). Indium tin oxide-coated microscope slides were purchased from Delta Technology (Loveland, CO). 4-(methylamino)cinnamic acid (MACA) and 4-(dimethylamino)cinnamic methyl ester (TMACA) were synthesized by the Vanderbilt Institute of Chemical Biology, Molecular Design, and Synthesis Center using a previously described methylation approach with ACA and DMACA as precursors for each product, respectively (Figs. S1 and S3) [11]. Proton nuclear magnetic resonance (NMR) spectroscopy was used to confirm the resulting structures of MACA and TMACA (Figs. S2 and S4).

2.2. Tissue sectioning

Mouse and rat brain tissues were purchased from BioIVT (Westbury, NY). Normal portions of human kidney tissue were collected through the Vanderbilt Cooperative Human Tissue Network as part of cancer-related total nephrectomies as part of the Human Biomolecular Atlas Program study. Murine and human tissues were flash frozen and stored at −80 °C [23,24]. Rat brain homogenate samples were prepared by sectioning 100 μm-thick sections of tissue into a Navy Lysis Kit Eppendorf (Next Advance, NY). A bullet blender tissue homogenizer (Next Advance, NY) was then used at maximum setting for 10 min. The resulting homogenate was then pipetted onto a metal plate cooled with dry ice (−78 °C) to form a homogenate bead ready for cryosectioning [25]. Human tissues were sectioned at 6 μm thickness and murine tissues and homogenate were sectioned at 10 μm thickness using a CM3050S cryostat from Leica Microsystems (GmbH, Wetzlar, Germany) and thaw mounted on

ITO-coated microscope glass slides. The tissue sections were then washed with 4 solutions of isotonic ammonium formate (150 mM) for 45 s in each solution and dried using nitrogen gas, followed by 20 min in a vacuum desiccator [26,27]. For long-term storage, the mounted tissue sections were vacuum sealed in a plastic bag and stored at −80 °C until used.

2.3. Spectroscopic measurements

Extinction coefficient measurements were performed at 355 nm using at SpectraMax M2 (Molecular Devices, San Jose, CA) (Fig. S5). In short, matrices were dissolved in tetrahydrofurane (THF) at 1 mg/mL and diluted to 10 μg/mL for measurement. 1 mL of each matrix solution was pipetted into a cuvette, and absorbance at 355 nm was acquired 3 times with at least 5 different concentrations for ACA, DMACA, DHA, and Nor. The extinction coefficients were then obtained using a simple linear regression of measurements collected using different concentration of each matrix. In solution absorption spectra were acquired for each matrix using a 10 μg/mL solution in THF (Fig. S6). The solid state spectra and absorption maxima of DMACA was obtained by sublimating the matrix into a quartz cuvette with an HTX sublimate (HTX Technologies, Chapel Hill, NC) using 1 mL of 1 mg/mL of the DMACA, following our standard sublimation protocol below (Fig. S7).

2.4. Matrix spraying

MALDI matrices were sprayed on the tissue sections using an M5 sprayer with a heated tray from HTX Technologies (Chapel Hill, NC) using either a 2:1 Acetone:ACN with 0.5 % dimethylformamide (DMF) for DAN or a 1:1:1 Acetone:ACN:THF with 0.5 % DMF for DMACA. The spray nozzle height was changed from 4 cm to 5 cm to accommodate a 1 cm pre-heated puck (130 °C). Optimal spray deposition conditions for individual matrices can be found in Supplemental Table 1. DAN (15 mg/mL) and DMACA (12 mg/mL) were sprayed on tissue for a final surface concentration of 0.85 and 0.68 μg/mm^2, respectively [28]. For ganglioside MALDI IMS, a modified decoupled spray method was use where a solution of ammonium sulfate at 8.25 mg/mL in 60 % ethanol was sprayed on the sample for a final density of 0.5 μg/mm^2 followed either DHA or ACA sprayed using pure organic solutions for a final density of 1.4 and 0.68 μg/mm^2 respectively as described above (Table S1).

2.5. Matrix sublimation

Sublimated samples were prepared using an in-house designed sublimation apparatus as described previously [29,30] and similar to the HTX sublimate platform (HTX Technologies, Chapel Hill, NC). In short, the prototype sublimation apparatus is filled with 2 mL (1 mL for HTX system) of matrix with concentrations varying between 2.5 and 20 mg/mL (solubilized in acetone), depending on the matrix. Complete sublimation of this matrix layer is then performed at 150-180 °C for 10–15 min at <200 mTorr onto the sample (Table S2). The final matrix surface densities can be found in Supplemental Table 3. Matrix surface concentrations were determined by weighing the tissue-mounted ITO slides before and after deposition of the matrices with the M5 sprayer or sublimation. The new proposed matrices undergo an additional step of thermal annealing where the slides are placed on a hot plate for 30s at 100 °C before analysis. For vacuum stability assessment, ITO slides were weighed before and after sublimation using an XSR104 balance (Mettler Toledo, Singapore) with a precision of 0.1 mg. Sublimation was performed using 1 mL of a 15 mg/mL solution producing a coating of 2–3 mg leading to a precision better than 5 % on the weight measurement. Sublimated slides were then exposed to the vacuum of a Bruker rapifleX mass spectrometer (source vacuum: 2×10^{-7} mbar) for at least 24h. The slides were then weighed again to measure matrix loss from high vacuum exposure (Table S4).

2.6. MALDI imaging mass spectrometry

Profiling and IMS measurements of thin tissue sections were performed on a Bruker MALDI timsTOF fleX mass spectrometer (Bruker Daltonics, Billerica, MA) in positive and negative ion mode [31]. Total laser power (TLP) refers to the actual percent output of the MALDI laser when considering the values of the global attenuator offset, attenuator offset, attenuator range, and final attenuator value set in flex control to obtain the true percent value of the laser being used. The optimal laser power for each matrix is defined as the maximum amount of laser power before oversampling occurs for a given raster size (Table S5). For 10 μm MALDI IMS experiments, 100 laser shots per pixel were used across all matrices, and 25 laser shots were used for 5 μm MALDI IMS experiments, both with a laser repetition rate of 10,000 Hz. Resulting ablation marks were evaluated using a H600L microscope (Nikon, Melville, NY) using a NIS-Elements AR 4.11.00 software (Fig. S8). DMACA ablation mark were also measured using scanning electron microscopy with a Zeiss Merlin (Zeiss, Wixom, MI) (Fig. S9). Data acquisition was performed using timsControl 5.1 and flexImaging 7.4 (Bruker Daltonics, Billerica, MA). Lipid identification was carried out by comparing accurate mass (≤2 ppm) with the LIPID MAPS [32] and/or HMDB [33] databases using in-house developed software along with accurate mass matching with LC-MS/MS data of tissue extracts as describe elsewhere [34,35]. The image pixel size (*i.e.,* pitch) was set to 5 or 10 μm, and laser spot size was confirmed to be less than 5 or 10 μm, respectively, at lower total laser power (Fig. S9), using either scanning electron microscopy (SEM) using a Zeiss Merlin (White Plains, NY) or brightfield microscopy with a Nikon Eclipse 90i microscope using a 40x objective (Nikon, Melville, NY). More detailed information for the instrumental parameters can be found in Fig. S10. Post-acquisition Periodic Acid-Schiff stain was performed following MALDI IMS using a series of ethanol washes as outlined in a previously established protocol [36].

2.7. Data analysis MALDI IMS data pre-processing

Data analysis was performed with DataAnalysis 5.3 (Bruker Daltonics, Billerica, MA). MALDI IMS visualization was performed using SCiLS lab 2023c Pro. Ion images are presented without normalization to allow for direct comparison of the raw intensity values (Figs. 1–3, S11-12) unless specifically stated otherwise in the figure captions (Fig. 4).

MALDI IMS data were exported from the Bruker timsTOF file raw format (.d) into a custom binary format. Each pixel/frame contained centroid peaks spanning the entire acquisition range. These were reconstructed into a pseudo-profile mass spectrum using Bruker's SDK (v2.21). The data were *m/z*-aligned using at least six peaks commonly present in the majority of pixels, utilizing the msalign library (v0.2.0) [37,38]. The mass axis of each dataset was calibrated using a minimum of four theoretical mass-to-charge values to achieve an accuracy of approximately ±1 ppm. For all analysis beyond simple ion image visualization, the MALDI IMS data were normalized using a total ion current (TIC) approach, and an average mass spectrum was computed based on all pixels (Figs. S13–15). The average mass spectrum was normalized between 0 and 1, peak picked, deisotoped, and filtered using an automatically established signal-to-noise (S/N) threshold. IMS peak annotation was performed using in-house developed software that associates detected peaks with tentative lipids identifications from the LIPID MAPS Structure Database (LMSD) and MSDIAL (V69) database. Parameters for annotating peaks include [M+H]+, [M+Na]+, and [M+K]+ adducts in positive, [M − H]- and [M-CH3]- adducts in negative mode, and a search window of ± 5 ppm. To provide more confident identification, IMS identifications were subsequently associated with LC-MS/MS identifications as well as reviewed against species reported in the literature.

Ion intensity comparisons were performed on average mass spectra using an equal number of pixels per sample (~4000 pixels). Tentatively identified ions were quantified by integrating signal within a ±2 mass bin window (total of 5 bins), capturing the majority of the peak. Bar

plots were generated using the Seaborn [39] library in Python, displaying mean ion intensity per matrix (ACA, DAN, DHA, DMACA) across three replicates, with error bars representing 95 % confidence intervals (Figs. S16–S17). For differential analysis, volcano plots were constructed by generating bootstrap distributions (n = 10,000) of ion intensities across replicates (Figs. S18–21). P-values were adjusted using the Benjamini-Hochberg false discovery rate (FDR) correction. Each volcano plot displays $\log_2$ (fold change) versus $-\log_{10}$ (adjusted p-value) for ion comparisons between matrices.

3. Results and discussion

3.1. Characterization of aminated cinnamic acid derivatives as MALDI matrices

We have developed a new family of dual polarity MALDI IMS matrices, which are vacuum stable, have high extinction coefficients at the wavelength generated by a triple Nd:YAG laser, are highly sensitive, have no known toxicity, and are affordable. Initially, IMS ion intensity and image quality were compared for the four aminated cinnamic acid derivative MALDI matrices using murine brain tissue. DMACA showed the highest signal intensity for phospholipids while ACA performed better for gangliosides, leading to better quality images for these molecular classes (Figs. S11–S12). While imaging performance is important in a MALDI matrix, vacuum stability is one of the most important physical properties for high spatial resolution MALDI IMS using intermediate pressure and high vacuum systems because of long image acquisition times. We thus assessed vacuum stability by measuring the mass of the slides coated in each matrix before and after storing them under vacuum for varying times (Table S4). For reference, DHA was also tested alongside as a commonly used dual polarity matrix. ACA, DMACA, and MACA were found to be vacuum stable for at least 48 h, even in a high vacuum ion source ($\sim 2 \times 10^{-7}$ mbar). The minor variation observed for these vacuum stable candidates (0.1 mg) was within the expected error of the balance, which is ±0.1 mg. TMACA was visibly gone after just 3 h inside the vacuum chamber, likely due to the increased volatility imparted by the esterification of the carboxylic acid functional group. Thus, TMACA was no longer considered for further experiments since both signal quality and vacuum stability was lacking compared to DMACA. DHA showed similar volatility to TMACA, largely subliming off after just a few hours.

Regarding an extinction coefficient at 355 nm, all aminated cinnamic acid derivatives presented high extinction coefficients at this wavelength in THF ($1\text{-}2\times10^4$ M^{-1} cm^{-1}, Table S6), particularly when compared to conventional MALDI matrices that display an order of magnitude worse extinction coefficients ($1\text{-}5\times10^3$ M^{-1} cm^{-1}), under similar conditions (Table S6 and Fig. S5). Even compared to the previously reported (E)-4-(2,5-dihydroxyphenyl)but-3-en-2-one (cDHA) and (E)-4-(4-hydroxy-3,5-dimethoxyphenyl)but-3-en-2-one (HDMP), which showed higher extinction coefficients at 355 nm than typical MALDI matrices, the aminated cinnamic acid MALDI matrices displayed particularly high absorptivity at 355 nm [10,40]. A high extinction coefficient can allow for the use of a substantially reduced laser power while maintaining efficient desorption and ionization during the MALDI process, which greatly reduces laser spot sizes at the sample surface, enabling higher spatial resolution analysis without oversampling. While the correlation between ionization threshold laser fluence and optical absorption is not necessarily linear [41], the high extinction coefficient of these aminated cinnamic acid derivatives does, in this case, promote ionization at laser energies far below what is possible with common MALDI matrices. This offers the practical advantage of enabling high spatial resolution MALDI IMS while maintaining good sensitivity.

Lipid IMS sensitivity of each of the aminated cinnamic acid analogs was assessed in negative ion mode using data collected from the hippocampus region of a mouse brain. DMACA performed better for phospholipids than ACA and MACA, most likely due to its higher extinction coefficient at 355 nm, enabling more efficient desorption/ionization (Fig. S13). On the other hand, ACA showed less in-source fragmentation of ganglioside species, allowing a more accurate molecular profile than DMACA or MACA for this class of molecules (Fig. S14). Higher order gangliosides are known to fragment easily, losing sialic acid residues, resulting in chemical structures that are the same as those of GM (mono-sialylated) gangliosides. As such, most MALDI experiments will show a higher abundance of GM species relative to GD (di-sialylated) and GT (tri-sialylated) lipids. However, compared to DMACA and MACA, ACA delivered a GM/GD ratio much closer to 1, a ratio known to be closer to reality in the murine brain [42]. Since DMACA exhibited better overall sensitivity and ACA minimized MALDI-induced ganglioside fragmentation, MACA was removed from further consideration in our study.

Image quality and sensitivity of DMACA and ACA were further compared to traditional lipid matrices DAN and DHA. Sagittal mouse brain tissue sections were imaged using 20 % total laser power, typical for conventional MALDI matrices such as DHA and DAN on the Bruker timsTOF flex platform. Overlays of five ion images and the overall average spectra for IMS experiments using DMACA, ACA, DAN, and DHA are shown in Fig. 1 and S15. An H&E-stained image is provided to provide histological context. The ion images were visualized together and without any intensity normalization to provide a direct qualitative comparison of the raw intensity for each of the selected ions. The highest intensity ions can be observed in all cases. For example, PI(38:4) (*m/z* 885.549, red) is the base peak for all the matrices tested, and its distribution is apparent in all cases. However, it is evident that DMACA and ACA are much more sensitive for SHexCer(42:1; O3) (*e.g., m/z* 906.633, green), and DMACA is the most sensitive overall across all selected ions with a 2–20 fold increase in intensity depending on the polarity and specific lipid species (Figs. S16–S17). Differential analysis comparing DMACA to DHA and DAN in both polarities found that most detected lipids exhibited a significant increase in intensity when using DMACA in all cases (Figs. S18–S21). In negative ion mode, DMACA was found to be more sensitive for 311 out of 336 and 293 out of 336 lipids compared to DHA and DAN, respectively. Similar results were observed in positive ion mode, with 147 out of 157 and 149 out of 157 lipids detected with higher intensity compared to DHA and DAN, respectively.

3.2. ACA vs. DHA for Ganglioside imaging

Gangliosides are a class of sialic acid-containing glycosphingolipids, which at high levels are primarily found in the central nervous system (CNS). They are typically anchored to the surface of the cell wall, where they are key for cell-to-cell communication by facilitating cell recognition, but they can also serve as receptors for protein interactions. IHC and MALDI IMS are the two predominant techniques used to study the spatial distribution of gangliosides. Recently, we developed a MALDI IMS sample preparation method using DHA for gangliosides, allowing for improved visualization while minimizing in-source fragmentation of higher order gangliosides [43,44]. Fig. 2 shows a direct comparison of ACA and DHA using this previously described decoupled matrix spray method. When comparing the average spectra from the MALDI IMS experiments collected from the hippocampus region of mouse brain tissue, we observe an increase in the intensity of di-sialylated (GD1) and tri-sialylated (GT1) gangliosides compared to the mono-sialylated species, suggesting reduction in MALDI-induced fragmentation when using ACA. Detecting that GDs are more abundant than GMs with ACA appears more aligned with previously reported LC-MS data from murine brain and it is likely a better representation of the actual ratio of these molecules in biological systems [42]. MALDI IMS experiments at 20 μm pixel sizes highlight the intensity disparity between ACA and DHA, where ACA consistently produces higher intensity signals for gangliosides than DHA, resulting in higher quality IMS images (Fig. S22). This can be seen in Fig. 2 where all gangliosides have higher intensity and image quality. This is especially the case for the highest order

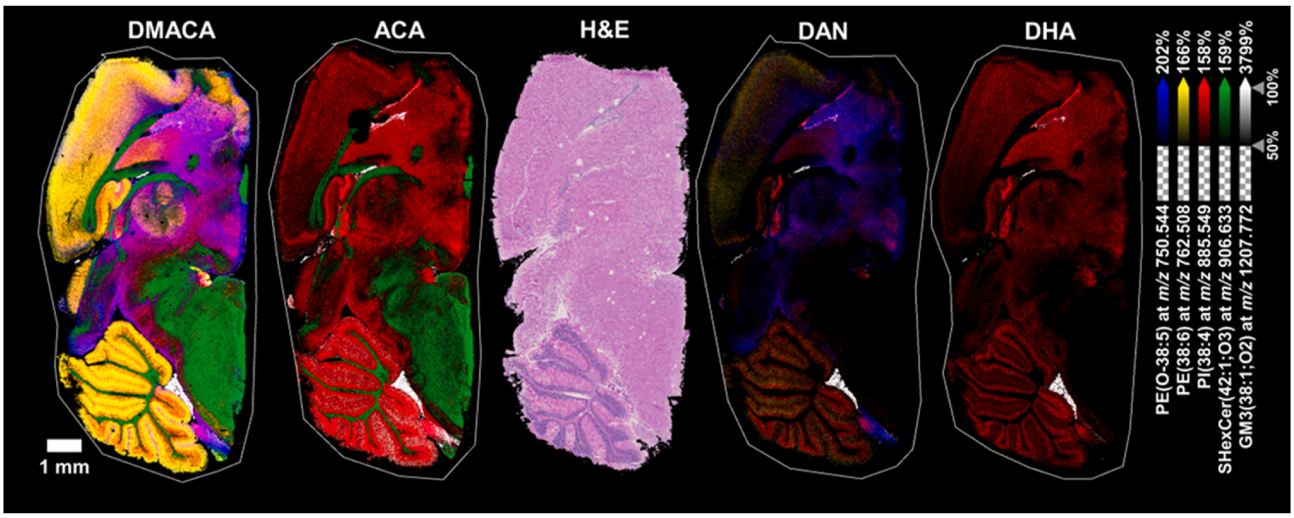

Fig. 1. MALDI IMS of lipids from 10 μm thick serial sections of a sagittal mouse brain section in negative ion mode, using sublimated DMACA, ACA, DAN, and DHA at 10 μm pixel sizes using a Bruker timsTOF fleX. Corresponding average mass spectra can be found in Fig. S5. In all signals but one (PS 40:6 @ *m/z* 834.529), DMACA and ACA performances were similar or superior to both DAN and DHA for phospholipid analysis at high spatial resolution. A post-acquisition H&E stained image from the DMACA experiment is displayed in the middle for histological reference. Ion images were thresholded to allow for better visualization of the higher intensity DMACA results. In all cases, every ion displayed was detected with every matrix, albeit with varying intensities.

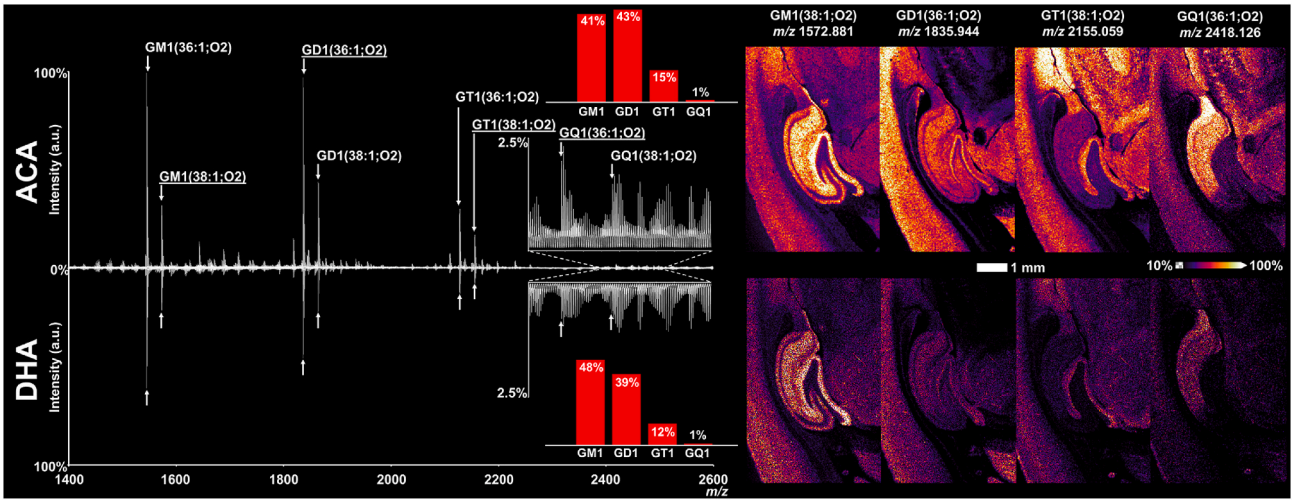

Fig. 2. MALDI IMS of gangliosides in the hippocampus region of a sagittal rat brain section in negative ion mode at 20 μm pixel size, using either ACA (top) or DHA (bottom) at 15.5 % TLP. The average spectra highlight the signal boost for gangliosides using ACA over DHA and suggest a better detected ratio of GM1 to GD1. Ion images for four typical ganglioside species show the higher quality measurements obtained through ACA (top row) and its ability to better resolve quadra-sialic acid ganglioside versus DHA (bottom row). The mass spectra are at the same intensity scale.

ganglioside detected, GQ1(36:1; O2) at *m/z* 2418.126, where the ion is only observed in the highest intensity regions of the tissue when using DHA, but ACA delivers a much more comprehensive and nuanced picture of its tissue distribution. With its ability to better reveal ganglioside distributions in brain tissue and its vacuum stability, ACA offers a new alternative to conventional MALDI matrices for the spatial elucidation of this important class of molecules in both normal and diseased tissues.

3.3. DMACA vs. DAN for high sensitivity dual polarity MALDI IMS

High-sensitivity MALDI matrices enable efficient desorption and ionization of targeted molecular classes at reduced laser energy, minimizing the resulting size of the focused laser beam on the sample surface and improving the feasibility of high spatial resolution imaging experiments. Since DMACA showed the greatest sensitivity during initial characterization, it was compared directly to DAN, a well-established, high-sensitivity MALDI matrix [11,16,20]. Fig. 3 shows ion images (10 μm pixel size) of human kidney tissue, generated using DAN and DMACA at various total laser powers. A total laser power of 20 % was chosen as it is the optimal setting for DAN using the MALDI timsTOF flex platform for 10 μm pixel size. Additionally, this was compared to a total laser power of 12.5 %, which was found to be the optimal setting for DMACA. At 20 % total laser power, both DAN and DMACA produce data of similar quality, but DMACA provides a ~2-fold increase in ion intensity for known lipid species (Figs. S23–S25). However, at a total laser power of 12.5 %, DMACA still produces high-quality ion images, whereas this is below the ionization threshold for DAN, resulting in no lipid ions. This dramatic reduction in laser energy concurrently reduces the laser beam diameter at the sample surface from ~6 μm at 20 % total laser power to ~4.5 μm at 12.5 % (Figures S9, S24-S26). Of course, sampling a smaller area does result in a slight reduction of signal (~2x), but even at lower energy and a significantly smaller sample ablation

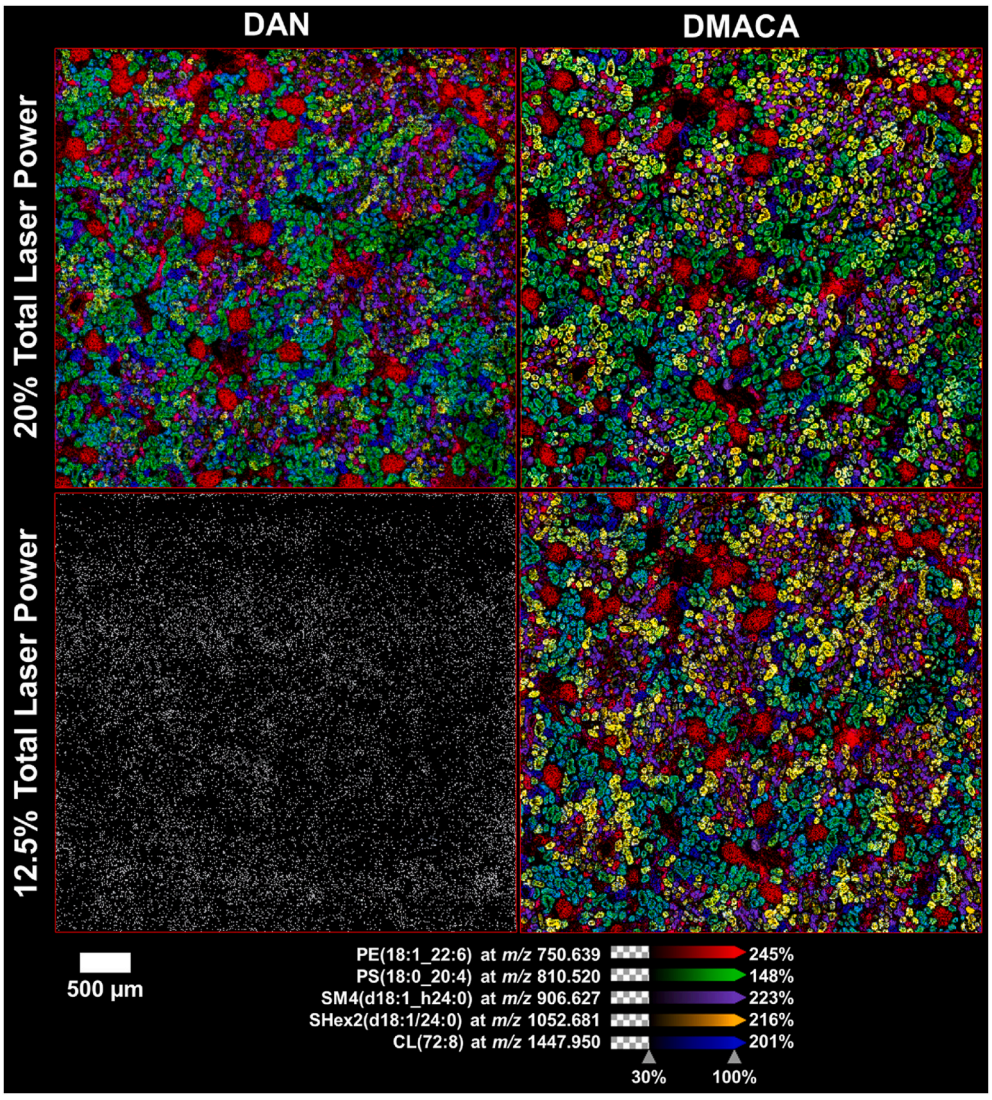

Fig. 3. MALDI IMS of a human kidney tissue section at 10 µm pixel size, using sprayed DAN and DMACA at their respective optimal laser powers. At a total laser power of 20 %, optimal for DAN, DMACA produces a higher quality MALDI IMS measurement, which results both in improved signal intensity and a lower amount of visible delocalization, compared to DAN's blurrier image. At 12.5 % TLP, DAN can no longer achieve proper desorption/ionization, while DMACA still offers high-quality IMS with ion intensity similar to that of DAN at 20 % TLP. Ion images were thresholded to allow better visualization of the higher intensity DMACA results. MALDI IMS with DAN did not yield any detectable signal for the low laser power experiment.

area, DMACA still produces data with an intensity similar to DAN at 20 % total laser power. Fig. S27 shows a similar experiment comparing DMACA and DHA, where DMACA also shows improved performance for negative mode phospholipids.

3.4. An optimized method for high resolution IMS with DMACA

MALDI IMS experiments are routinely performed using automated pneumatic sprayers and sublimation apparatuses for matrix application. Both approaches have advantages and disadvantages, but sublimation is often preferable for high spatial resolution imaging experiments, given the low micrometer scale matrix crystals that are often produced by the sublimation process. Vacuum stable matrices can sometimes be challenging to sublimate, requiring higher vacuum and/or temperature compared to more volatile compounds. To explore the capability of aminated cinnamic acid analogs for high resolution imaging using sublimation, DMACA was subjected to various sublimation conditions [16,22,29]. 'Thin' sublimated layers of DMACA (~0.22 µg/mm^2) produced a semi-transparent, iridescent matrix film that led to low ion signals compared to thicker layers (0.5–1.0 µg/mm^2), which are more typical for MALDI IMS experiments. When analyzed by scanning electron microscopy, the resulting sublimated thin layer showed no visible crystals on the tissue (Fig. S28). This observation suggested that when applied by sublimation, the matrix is amorphous, which indicated that the matrix sublimation method might benefit from re-crystallization.

Re-crystallization in MALDI IMS workflows is often performed using a variety of solvent compositions through a custom-made vapor chamber [45,46]. However, solvent-based recrystallization methods can lead to analyte delocalization in most cases. To overcome this challenge, we developed a simple solvent-free approach using only heat to induce crystallization (*i.e.,* heat annealing) of the amorphous matrix layer. Fig. S28 shows scanning electron microscopy images of the matrix layer before and after heat annealing. The heat annealing method is performed by placing the matrix-coated slide on a hot plate (100 °C) for 30s. Heat annealing led to a clear change in the coloration, a conversion from a transparent to opaque thin matrix layer, indicating a change to the optical properties of the surface (Fig. S29). Scanning electron microscopy images show this change in the transition from a crystal-free layer to a crystalline layer with crystal sizes ranging from 200 to 500 nm after heat annealing (Fig. S28). This process was also tested with conventional

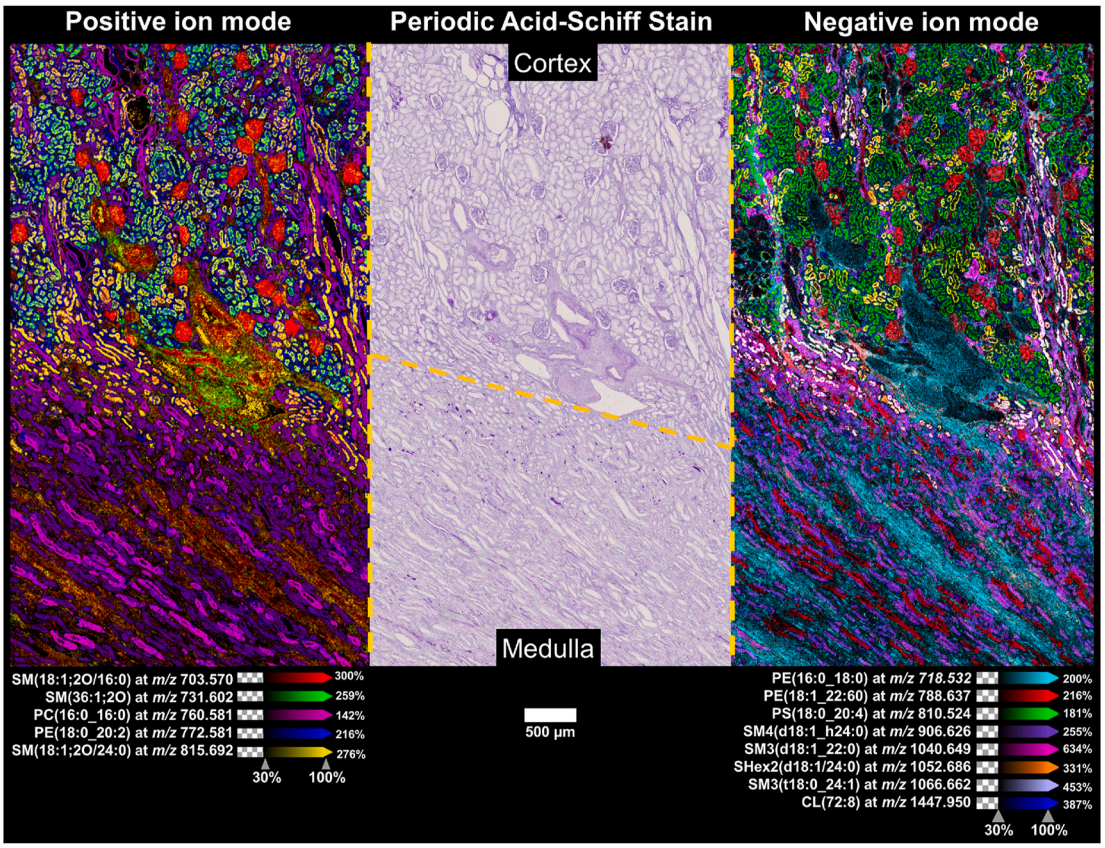

Fig. 4. MALDI IMS measurements of 6 µm thick serial sections of a human kidney sample at 5 µm pixel size, using sublimated DMACA as the matrix in both positive (left) and negative (right) ion mode. Both positive and negative modes highlight the complex structure of the human kidney, with the cortex region at the top, where glomeruli can be visualized in red, and the medulla region at the bottom. A post-acquisition PAS stain of the negative mode experiment is presented in the middle for histological reference. Images were normalized using total ion current. (For interpretation of the references to color in this figure legend, the reader is referred to the Web version of this article.)

MALDI matrices, such as DHA and DAN, but was found not to work due to the volatility of these matrices. Both matrices sublimated from the slide at atmospheric pressure, either completely (DHA) or partially (DAN), in the fume hood while attempting heat annealing. This heat annealing process increases ion signals by roughly 2-to-3-fold compared to methods without recrystallization (Figs. S30–S31). Moreover, sublimation of DMACA, followed by annealing, was also found to be more sensitive than matrix spraying methods, without the risk of delocalization, for high spatial resolution experiments. (Figs. S30–S31). Both observations are tissue type, molecular class, and matrix dependent. It is noted that we did not observe any thermal degradation of endogenous molecules from the short annealing process, but further studies are needed to assess this across a wider range of molecular classes.

With this optimized method, we demonstrated the capability for mapping lipids at high spatial resolution collecting MALDI IMS data from a fresh-frozen human kidney tissue section using 5 µm pixels, which is the practical limit for most commercial mass spectrometers at the time of writing. Fig. 4 shows selected ion images for both positive (5 lipid species) and negative (8 lipid species) ion modes. A periodic acid-Schiff (PAS)-stained image (stained after MALDI acquisition) is included for reference to highlight the histology of the tissue (Fig. S32). For both polarities, ions reported as red represent glomeruli, while green-reported ion species delineate proximal tubules, which are only found in the cortex region of the kidney. Lipids associated with the proximal tubules and descending limb are colored in orange, while those colored purple were observed in the ascending limb of the nephron. These span from the cortex to the medulla of the kidney. It is noted that these assignments to specific components of the nephron are made possible by the high-quality PAS-stained images that can be acquired post-MALDI IMS-acquisition using this method. In addition to enabling smaller IMS pixel sizes, the lower laser energy also induces less tissue damage during irradiation, improving performance for subsequent microscopy modalities as part of multimodal studies [47,48]. Along with these selected ion signals, we annotated ~300 lipids, of which ~120 lipids were found in positive ion mode and ~180 in negative ion mode at 5 µm pixel size. While the number of total ions detected is lower than typically observed at 10 µm pixel size in human kidney, these data showcase the advantages of DMACA for high spatial resolution MALDI IMS. The performance of this method allows for spatial heterogeneity to be observed for most ions, even within individual components of the nephron, including individual glomeruli (Fig. S33). This highlights the capacity of DMACA and our optimized matrix application method for providing the sensitivity necessary to produce ion images at cellular resolution without the need for custom instrumental setups.

4. Conclusions

In conclusion, we have developed a new family of dual polarity MALDI matrices that are vacuum stable, have a high extinction coefficient at 355 nm (1-2 × 10^4 $M^{-1}cm^{-1}$), are highly sensitive for lipid and metabolite imaging, have no known toxicity for humans, and are affordable. This new matrix family is derived from 4-amino cinnamic acid with up to 3 sequential methylation events to tailor their optical properties. Among the four analogs studied, ACA and DMACA emerged as the most promising, minimizing MALDI-induced fragmentation while enhancing sensitivity for high spatial resolution MALDI IMS. ACA was found to be a 'soft' matrix, exhibiting the lowest level of in-source fragmentation, which is ideal for the analysis of thermally labile

molecules, such as gangliosides. DMACA offered the highest sensitivity for phospholipids and sulfatides, with both matrices requiring lower laser power for efficient desorption and ionization than common MALDI matrices such as DAN and DHA.

High spatial resolution was achieved with both matrices (<10 μm pixel size), with DMACA enabling imaging with 5 μm pixels on tissue without oversampling or significant sacrifice to signal quality when optimized on appropriate instrumentation. Complementary microscopy showed that this was achievable while, at the same time, minimizing tissue damage during laser irradiation. These advancements can enhance the overall performance of commercial MALDI imaging platforms and substantially boost support for advanced multimodal workflows. More broadly, the improved sensitivity, spatial resolution, and stability of this new matrix family have the potential to expand the scope and ease-of-use of MALDI IMS in biological and biomedical research. By enabling more robust and precise molecular mapping of tissue microenvironments, these matrices will facilitate deeper insights into cellular metabolism, lipid dysregulation, and biomarker discovery. Their ability to preserve tissue integrity with enhanced detection sensitivity, even at high spatial resolution, will be particularly valuable for MALDI IMS studies that aim to link untargeted molecular profiles to specific tissue features, cell types, and eventually single cells *in situ*. Collectively, this new matrix family provides a powerful toolset for advancing molecular imaging applications and driving biological discoveries.

CRediT authorship contribution statement

Martin Dufresne: Writing – review & editing, Writing – original draft, Visualization, Validation, Project administration, Methodology, Formal analysis, Data curation, Conceptualization. **Lukasz G. Migas:** Writing – review & editing, Writing – original draft, Visualization, Software, Formal analysis, Data curation. **Katerina V. Djambazova:** Writing – review & editing, Writing – original draft, Methodology, Investigation, Formal analysis. **Madeline E. Colley:** Writing – review & editing, Writing – original draft, Validation, Formal analysis, Data curation. **Raf Van de Plas:** Writing – review & editing, Supervision, Software, Resources, Methodology, Formal analysis. **Jeffrey M. Spraggins:** Writing – review & editing, Writing – original draft, Supervision, Resources, Methodology, Funding acquisition, Formal analysis, Conceptualization.

Declaration of competing interest

The authors declare the following financial interests/personal relationships which may be considered as potential competing interests: Jeffrey Spraggins and Raf Van de Plas reports financial support was provided by National Institute of Health. Lukasz Migas and Raf Van de Plas reports financial support was provided by The Chan Zuckerberg Initiative. Jeffrey Spraggins reports financial support was provided by National Science Foundation. If there are other authors, they declare that they have no known competing financial interests or personal relationships that could have appeared to influence the work reported in this paper.

Acknowledgments

This work was supported by the National Institutes of Health (NIH) Common Fund and National Institute Of Diabetes And Digestive And Kidney Diseases (NIDDK) under Award Numbers U54DK134302 and U01DK133766 (J M S. and R.V.), by the NIH National Institute On Aging (NIA) under Award Number R01AG078803 (J M S. and R.V.), and by the National Science Foundation Major Research Instrument Program CBET – 1828299 (J.M.S.). This research was furthermore made possible by the Chan Zuckerberg Initiative DAF, an advised fund of the Silicon Valley Community Foundation, under Award Numbers 2021–240339 and 2022–309518 (L G M. and R.V.). K.V.D was supported by an NIDDK training grant (T32DK007569-34). The content is solely the responsibility of the authors and does not necessarily represent the official views of the funders. The authors would like to thank Jamie Allen for processing and preparing frozen tissue blocks of human kidney tissue. The Vanderbilt Institute of Nanoscale Science and Engineering performed scanning electron microscopy measurements, and the Vanderbilt Institute of Chemical Biology, Molecular Design, and Synthesis Center provided ACAA compounds.

Appendix A. Supplementary data

Supplementary data to this article can be found online at https://doi.org/10.1016/j.aca.2025.344423.

Data availability

Data will be made available on request.

References

[1] R.M. Caprioli, T.B. Farmer, J. Gile, Molecular imaging of biological samples: localization of peptides and proteins using MALDI-TOF MS, Anal. Chem. 69 (1997) 4751–4760, https://doi.org/10.1021/ac970888i.
[2] H.B. Taylor, et al., Tissue proteomics: methods and protocols. Taufika Islam Williams, Springer US, 2025, pp. 305–332.
[3] H. Zhang, et al., Mass spectrometry imaging for spatially resolved multi-omics molecular mapping, npj Imaging 2 (2024) 20, https://doi.org/10.1038/s44303-024-00025-3.
[4] D.R. Klein, E.S. Rivera, R.M. Caprioli, J.M. Spraggins, Imaging mass spectrometry of isotopically resolved intact proteins on a trapped ion-mobility quadrupole time-of-flight mass spectrometer, Anal. Chem. 96 (2024) 5065–5070, https://doi.org/10.1021/acs.analchem.3c05252.
[5] F. Xie, T. Gales, M.A. Ringenberg, A.I. Wolf, M.R. Groseclose, Characterizing the distribution of a stimulator of interferon genes agonist and its metabolites in mouse liver by matrix-assisted laser desorption/ionization imaging mass spectrometry, Drug Metabol. Dispos. 52 (2024) 1181–1186, https://doi.org/10.1124/dmd.122.001076.
[6] M. Niehaus, J. Soltwisch, M.E. Belov, K. Dreisewerd, Transmission-mode MALDI-2 mass spectrometry imaging of cells and tissues at subcellular resolution, Nat. Methods 16 (2019) 925–931, https://doi.org/10.1038/s41592-019-0536-2.
[7] M. Aichler, A. Walch, MALDI Imaging Mass Spectrometry: Current Frontiers and Perspectives in Pathology Research and Practice, vol. 95, Laboratory Investigation, 2015, pp. 422–431, https://doi.org/10.1038/labinvest.2014.156.
[8] M. Dufresne, N.H. Patterson, J.L. Norris, R.M. Caprioli, Combining salt doping and matrix sublimation for high spatial resolution MALDI imaging mass spectrometry of neutral lipids, Anal. Chem. (2019), https://doi.org/10.1021/acs.analchem.9b02974.
[9] Q. Zhou, A. Fülöp, C. Hopf, Recent developments of novel matrices and on-tissue chemical derivatization reagents for MALDI-MSI, Anal. Bioanal. Chem. 413 (2021) 2599–2617, https://doi.org/10.1007/s00216-020-03023-7.
[10] J. Yang, J.L. Norris, R. Caprioli, Novel vacuum stable ketone-based matrices for high spatial resolution MALDI imaging mass spectrometry, J. Mass Spectrom. 53 (2018) 1005–1012, https://doi.org/10.1002/jms.4277.
[11] P. Huang, et al., Toward the rational design of universal dual polarity matrix for MALDI mass spectrometry, Anal. Chem. 92 (2020) 7139–7145, https://doi.org/10.1021/acs.analchem.0c00570.
[12] M.E. Colley, A.B. Esselman, C.F. Scott, J.M. Spraggins, High-specificity imaging mass spectrometry, Annu. Rev. Anal. Chem. 17 (2024) 1–24, https://doi.org/10.1146/annurev-anchem-083023-024546.
[13] M. Yang, et al., Nano-DESI mass spectrometry imaging of proteoforms in biological tissues with high spatial resolution, Anal. Chem. 95 (2023) 5214–5222, https://doi.org/10.1021/acs.analchem.2c04795.
[14] S. Ma, et al., High spatial resolution mass spectrometry imaging for spatial metabolomics: advances, challenges, and future perspectives, TrAC, Trends Anal. Chem. 159 (2023) 116902, https://doi.org/10.1016/j.trac.2022.116902.
[15] K.V. Djambazova, J.M. Van Ardenne, J.M. Spraggins, Advances in imaging mass spectrometry for biomedical and clinical research, TrAC, Trends Anal. Chem. 169 (2023) 117344, https://doi.org/10.1016/j.trac.2023.117344.
[16] A. Thomas, J.L. Charbonneau, E. Fournaise, P. Chaurand, Sublimation of new matrix candidates for high spatial resolution imaging mass spectrometry of lipids: enhanced information in both positive and negative polarities after 1,5-Diaminonapthalene deposition, Anal. Chem. 84 (2012) 2048–2054, https://doi.org/10.1021/ac2033547.
[17] X. Lin, C. Xiao, L. Ling, L. Guo, X. Guo, A dual-mode reactive matrix for sensitive and quantitative analysis of carbohydrates by MALDI-TOF MS, Talanta 235 (2021) 122792, https://doi.org/10.1016/j.talanta.2021.122792.
[18] X. Wang, et al., Hydroxyflavones as a new family of matrices for MALDI tissue imaging, Anal. Chem. 85 (2013) 7566–7573, https://doi.org/10.1021/ac401595a.
[19] T. Yamagaki, H. Nakanishi, A new technique distinguishing α2-3 sialyl linkage from α2-6 linkage in sialyllactoses and sialyl-N-acetyllactosamines by post-source

decay fragmentation method of MALDI-TOF mass spectrometry, Glycoconj. J. 16 (1999) 385–389, https://doi.org/10.1023/A:1007050909293.
[20] A.J. Scott, et al., Mass spectrometry imaging enriches biomarker discovery approaches with candidate mapping, Health Phys. 106 (2014) 120–128, https://doi.org/10.1097/HP.0b013e3182a4ec2f.
[21] A.J. Scott, et al., Norharmane matrix enhances detection of endotoxin by MALDI-MS for simultaneous profiling of pathogen, host, and vector systems, Pathog Dis 74 (2016), https://doi.org/10.1093/femspd/ftw097.
[22] L.R.S. Huizing, et al., Development and evaluation of matrix application techniques for high throughput mass spectrometry imaging of tissues in the clinic, Clin Mass Spectrom 12 (2019) 7–15, https://doi.org/10.1016/j.clinms.2019.01.004.
[23] M.P. Snyder, et al., The human body at cellular resolution: the NIH human biomolecular atlas program, Nature 574 (2019) 187–192, https://doi.org/10.1038/s41586-019-1629-x.
[24] S. Jain, et al., Advances and prospects for the human BioMolecular atlas program (HuBMAP), Nat. Cell Biol. 25 (2023) 1089–1100, https://doi.org/10.1038/s41556-023-01194-w.
[25] M.R. Groseclose, S. Castellino, A mimetic tissue model for the quantification of drug distributions by MALDI imaging mass spectrometry, Anal. Chem. 85 (2013) 10099–10106, https://doi.org/10.1021/ac400892z.
[26] H.-Y.J. Wang, C.B. Liu, H.-W. Wu, A simple desalting method for direct MALDI mass spectrometry profiling of tissue lipids, JLR (J. Lipid Res.) 52 (2011) 840–849, https://doi.org/10.1194/jlr.D013060.
[27] P.M. Angel, J.M. Spraggins, H.S. Baldwin, R. Caprioli, Enhanced sensitivity for high spatial resolution lipid analysis by negative ion mode matrix assisted laser desorption ionization imaging mass spectrometry, Anal. Chem. 84 (2012) 1557–1564, https://doi.org/10.1021/ac202383m.
[28] M. Dufresne, A.R.S. Kruse, J. Allen, D. Gutierrez, J.M. Spraggins, Deposition of mastrix using an M5 TM sprayer for high resolution MALDI analysis. https://www.protocols.io/view/deposition-of-matrix-using-an-m5-tm-sprayer-for-hi-cse3wbgn.html, 2023.
[29] J.A. Hankin, R.M. Barkley, R.C. Murphy, Sublimation as a method of matrix application for mass spectrometric imaging, J. Am. Soc. Mass Spectrom. 18 (2007) 1646–1652, https://doi.org/10.1016/j.jasms.2007.06.010.
[30] D. Anderson, et al., Matrix sublimation via In-House developed sublimation apparatus. https://www.protocols.io/view/matrix-sublimation-via-in-house-developed-sublimat-n92ldpyn9l5b/v1, 2023.
[31] J.M. Spraggins, et al., High-performance molecular imaging with MALDI trapped ion-mobility time-of-flight (timsTOF) mass spectrometry, Anal. Chem. 91 (2019) 14552–14560, https://doi.org/10.1021/acs.analchem.9b03612.
[32] M. Sud, et al., LMSD: LIPID MAPS structure database, Nucleic Acids Res. 35 (2007) D527–D532, https://doi.org/10.1093/nar/gkl838.
[33] D.S. Wishart, et al., Hmdb 4.0: the human metabolome database for 2018, Nucleic Acids Res. 46 (2018) D608–D617, https://doi.org/10.1093/nar/gkx1089.
[34] A.B. Esselman, et al., In situ molecular profiles of glomerular cells by integrated imaging mass spectrometry and multiplexed immunofluorescence microscopy, Kidney Int. 107 (2025) 332–337, https://doi.org/10.1016/j.kint.2024.11.008.
[35] M.E. Colley, et al., Bulk untargeted LC-MS/MS lipidomics. https://www.protocols.io/view/bulk-untargeted-lc-ms-ms-lipidomics-ewov1ob5klr2/v1, 2023.
[36] E. Neumann, et al., PAS staining of fresh frozen or paraffin embedded human kidney tissue. https://www.protocols.io/view/pas-staining-of-fresh-frozen-or-paraffin-embedded-cpxtvpnn, 2023.
[37] P. Monchamp, L. Andrade-Cetto, J.Y. Zhang, R. Henson, Signal processing methods for mass spectrometry. Systems Bioinformatics: an Engineering Case-based Approach, Artech House Publishers, 2007.
[38] L.G. Migas, Spectral alignment based on MATLAB's 'msalign' function. https://github.com/lukasz-migas/msalign, 2024.
[39] M.L. Waskom, Seaborn: statistical data visualization, J. Open Source Softw, 6 (60) (2021) 3021, https://doi.org/10.21105/joss.03021.
[40] H. Kettling, et al., MALDI mass spectrometry imaging of bioactive lipids in mouse brain with a synapt G2-S mass spectrometer operated at elevated pressure: improving the analytical sensitivity and the lateral resolution to ten micrometers, Anal. Chem. 86 (2014) 7798–7805, https://doi.org/10.1021/ac5017248.
[41] K.N. Robinson, R.T. Steven, J. Bunch, Matrix optical absorption in UV-MALDI MS, J. Am. Soc. Mass Spectrom. 29 (2018) 501–511, https://doi.org/10.1007/s13361-017-1843-4.
[42] S. Ando, in: Neville N. Osborne (Ed.), Selected Topics from Neurochemistry, Pergamon, 1985, pp. 439–486.
[43] K.V. Djambazova, et al., MALDI TIMS IMS of disialoganglioside Isomers—GD1a and GD1b in murine brain tissue, Anal. Chem. 95 (2023) 1176–1183, https://doi.org/10.1021/acs.analchem.2c03939.
[44] K.V. Djambazova, et al., MALDI TIMS IMS reveals ganglioside molecular diversity within murine S. aureus kidney tissue abscesses, J. Am. Soc. Mass Spectrom. 35 (2024) 1692–1701, https://doi.org/10.1021/jasms.4c00089.
[45] J. Yang, R.M. Caprioli, Matrix sublimation/recrystallization for imaging proteins by mass spectrometry at high spatial resolution, Anal. Chem. 83 (2011) 5728–5734, https://doi.org/10.1021/ac200998a.
[46] W. Bouschen, O. Schulz, D. Eikel, B. Spengler, Matrix vapor deposition/recrystallization and dedicated spray preparation for high-resolution scanning microprobe matrix-assisted laser desorption/ionization imaging mass spectrometry (SMALDI-MS) of tissue and single cells, Rapid Commun. Mass Spectrom. 24 (2010) 355–364, https://doi.org/10.1002/rcm.4401.
[47] A.B. Esselman, et al., Microscopy-directed imaging mass spectrometry for rapid high spatial resolution molecular imaging of glomeruli, J. Am. Soc. Mass Spectrom. 34 (2023) 1305–1314, https://doi.org/10.1021/jasms.3c00033.
[48] A.B. Esselman, et al., A streamlined workflow for microscopy-driven MALDI imaging mass spectrometry data collection, J. Am. Soc. Mass Spectrom. 35 (2024) 2795–2800, https://doi.org/10.1021/jasms.4c00365.